**RESEARCH ARTICLE**

# Novel polymeric zinc phthalocyanine for electro-oxidation and detection of ammonia

C. P. Keshavananda Prabhu[1] · Shambhulinga Aralekallu[1] · Manjunatha Palanna[1] · Veeresh Sajjan[1] · B. Renuka[1] · Lokesh Koodlur Sannegowda[1]

## Abstract

The design and development of new catalysts with low cost, high selectivity, and sensitivity for the electrochemical sensor applications is of huge interest. In this report, novel zinc tetra [4-[2-(1H-benzimidazol-2-yl) phenoxy]] phthalocyanine (ZnTBImPc) is prepared in a pure state with 87% yield. The characterization of the ligands and complex is carried out by combination of techniques like elemental analysis, ultraviolet–visible (UV–Vis), Fourier-transform infrared spectroscopy (FTIR), mass spectral, thermogravimetric analysis (TGA), X-ray diffraction (XRD), and electrochemical techniques. FTIR is useful in monitoring the progress of the reaction. The benzimidazole moiety of ZnTBImPc undergoes electropolymerization and thin, uniform polymeric layer deposits on the glassy carbon surface. The polymeric film was characterized by impedance spectra and charge transfer studies. The fabricated polymeric film electrode is applied for voltammetric sensing of ammonia which showed linear characteristics in 0.1 to 1.0 µM concentration range. The LOD was 30 nM with sensitivity of 237.25 µA µM$^{-1}$ cm$^{-2}$. The efficiency and sensitivity of ammonia oxidation at the poly(ZnTBImPc) are compared with the composite hybrid electrode of poly(ZnTBImPc) and carbon nanoparticle (CNP). The amperometric sensing of ammonia showed linear behavior in 50 to 500 nM concentration range. The RDE experiment revealed that the number of electrons involved in the ammonia oxidation is nearly 3. The polymeric electrode was subjected to the interference studies to evaluate the selectivity of the fabricated electrode and found that the co-existing molecules do not show interference during the detection of ammonia.

**Graphical abstract**

Schematic representation of electro-oxidation and detection of ammonia
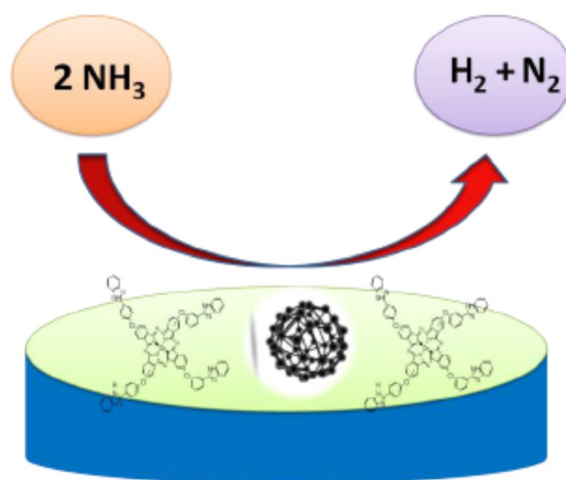
Extended author information available on the last page of the article

# 1 Introduction

Ammonia is a pungent-smelled colorless gas which is amphoteric in nature and extremely soluble in water. The main source of ammonia is the excreta of animals/birds. In addition, ammonia is one of the major micro-nutrients in the fertilizers like di-ammonium phosphate (DAP). DAP fertilizer contains phosphorus (P) and nitrogen (N) which are very essential for plant growth [1, 2]. DAP is highly soluble and dissolves quickly in soil to discharge the required phosphate and ammonium to soil. Ammonia forms fog at elevated concentration (16–25% by wt in air) and catches fire. Because of this feature, ammonia is also used in rocket as propellant in smaller amount. It has enormous applications in industrial, automotive, and medical fields [3].

Ammonia is a building block for many commercial cleaning products [4]. In general, ammonia solutions are used to clean, bleach, and deodorize. It has also been used as refrigerant gas, explosive, water purification, textiles, pesticides, and others. But it is toxic, when exposed to higher concentration in the atmosphere and leads to the burning of the respiratory tract and other body organs like eyes, nose, and even it can result in lung damage (or) to death. Intake of lower concentration of ammonia may lead to cough, nose, and throat infection. Elevated ammonia level in the blood results in liver failure [1, 5]. Hence, it is very essential to monitor the amount of ammonia in the atmosphere or various samples. Among the various methods developed to detect ammonia, electrochemical methods are simple, reliable, and sensitive. But the electrocatalytic reduction of ammonia is slow and requires higher overpotential at pristine electrodes. Therefore, modification of the electrode with a suitable electron mediator is essential to enhance the charge transfer. Various macrocycles, polymers, nanoparticles, metal oxides, etc., have been used as electron mediators [6–12]. Recently, phthalocyanine-based macrocycles have been extensively used as electrocatalysts for various electrochemical applications [7].

The phthalocyanine macrocycles have clinched great attention in recent years due to their unique chemical, photochemical, thermal stability, and coordination properties and improved optical characteristics. They find applications in dyes and pigments and, in addition, have been recently studied extensively as efficient materials in catalysis [7], non-linear optics, chemical sensors, nanotechnology [8], and photodynamic cancer therapy (PDT) [9].

These applications require the smart modification of the phthalocyanine macrocycle to yield molecules with the targeted properties. For example, photosensitizers for photodynamic therapy (PDT) in treatment of cancer require Pc molecules with diamagnetic ions such as Zn(II) because of their ability to generate high singlet oxygen ($^1O_2$) yield which is toxic for tumor cells [10]. Furthermore, the PDT properties of the phthalocyanines are strongly influenced by the substituents introduced on the periphery of the Pcs.

Benzimidazole derivatives are a very important class of nitrogen-containing aromatic heterocyclic compounds. They possess interesting physico-chemical properties and a wide range of applications in various domains [9]. The benzimidazole derivatives are extensively studied as organic fluorescent chromophores. Fluorescence characteristic of these compounds can be altered with substitution of different groups at –NH position of benzimidazole skeleton. Benzimidazole compounds have also been commonly used in molecular recognition of cations, anions, and neutral molecules [11].

The combination of the functional groups with the core Pc structure is a challenging work in molecular engineering. In view of the electrochemical importance and activities of both benzimidazoles and phthalocyanines, the construction of multicomponent system involving these functional structures is considered as complementary systems with excellent molecular architecture resulting in potential electrochemical activities for sensing applications.

Thus, ZnPc-containing benzimidazole groups through oxygen bridges have been synthesized as new functionalized materials. The analytical and electrochemical studies of benzimidazole group-substituted Pc complexes are presented. Further, in order to exploit their unique properties for electrochemical application, they are modified on the electrode surface. Compared to other modification techniques, electropolymerization is highly beneficial as it provides thin, uniform, and better interaction between electrode and polymeric film and which in turn reduces the interfacial resistance and enhances the charge transfer. In addition, the electropolymerization extends the conjugation and conductivity. Further, the electroactivity of the MPcs can be enhanced by designing hybrid composite of Pc with graphene, carbon nanotube, and/or carbon nanoparticles [6, 13]. Hybrid material plays an important role due to the synergic effects of the electrical, optical, or mechanical properties of the 2 components [7, 14–16]. The use of carbon nanoparticles for sensing has been of great interest due to their promising and unique properties like high surface-volume ratio and sensitive electronic properties [17–22].

In the present work, zinc tetrabenzimidazole phthalocyanine macrocycle was successfully synthesized and electropolymerized on surface of the electrode. The polymeric layer was utilized in the amperometric sensing of ammonia, and the results were compared with the hybrid composite of polymeric Pc with carbon nanoparticles.

## 2 Experimental section

### 2.1 Materials

Various chemicals used for synthesis and electrochemical studies are presented in Table 1 with their purity and used as such without any further purification.

### 2.2 Synthesis of 2-(1H-benzimidazol-2-yl) phenol precursor (i)

The precursor (**i**) was prepared by mixing o-phenylenediamine (5 g, 0.0461 mol) and Salicylic acid (6.35 g) in a RB flask with 50 mL 4 N HCl and 5 mL $H_2SO_4$ and refluxed at 140–150 °C for about 8 h. The crude product was cooled, and ice pieces were added to accelerate the cooling. The crude compound was neutralized by using sodium bicarbonate and filtered. The product was washed with methanol and dried.

Yield: 90%. Melting point: 158 °C. Anal. for the compound (**i**), mol. wt 210.23. $C_{13}H_{10}N_2O$: Calc. (%) C, 74.20; H, 4.75; N, 13.31; O, 7.61. Found (%): C, 74.52; H, 4.52; N, 13.05. FTIR bands (KBr (pellet), $cm^{-1}$): 742, 807, 1191, 1208, 1247, 1312, 1428, 1544, 1240, 1620, 3100, and 3400. Mass: 211 ($M^{+1}$).

### 2.3 Synthesis of 4-[2-(1H-benzimidazol-2-yl) phenoxy] benzene-1, 2-dicarbonitrile ligand (ii)

Ligand (**ii**) was prepared by combining precursor (**i**) (2 g, 0.0095 mol), 4-nitrophthalonitrile (1.648 g, 0.0095 mol), and potassium carbonate (1.3161 g, 0.0095 mol) in RB flask containing 30 mL DMF and stirred at ambient condition for 1 day. Then the product was transferred into cold water, and the crude product was filtered, washed with water, and dried. The compound was recrystallized in methanol.

Yield: 92%. Melting point: 138 °C. Anal. for the compound (**ii**), mol. wt 336.34. $C_{21}H_{12}N_4O$: Calc. (%) C, 74.92; H, 3.56; N, 16.64; O, 4.78. Found (%): C, 74.52; H, 3.23; N, 16.94. FTIR bands (KBr (Potassium bromide) pellet, $cm^{-1}$): 742, 807, 910, 1091, 1208, 1247, 1312, 1428, 1504, 1540, 2242, 2950, and 3100. $^1$H-NMR (400 MHz, DMSO-$d_6$): $\delta$ 5.40 (s, 1H), 6.75 (d, J = 6.00 Hz, 2H), 6.84 (d, J = 8.00 Hz, 2H), 7.06 (d, J = 8.00 Hz, 2H), 7.25–7.27 (m, 4H). Mass: 334 ($M^{-2}$).

### 2.4 Synthesis of zinc tetra [4-[2-(1H-benzimidazol-2-yl) phenoxy]] phthalocyanine (ZnTBImPc) (iii)

The mixture of ligand (**ii**) (1 g, 0.00192 mol), zinc acetate (0.1 g, 0.0002 mol), 1-pentanol (20 mL), and a catalytic amount of 1,8-Diazabicyclo[5.4.0]undec-7-ene (DBU) were charged into a 100 mL RB flask and refluxed with a constant stirring at 140 °C for 24 h. The green-colored compound

**Table 1** Various chemicals used in this work, purity, and their make

| Reagents | Purity | Make | Chemical formula |
|---|---|---|---|
| Zinc acetate | 99.99% | Alfa-aesar | $Z_nC_4H_6O_4$ |
| O-Phenylenediamine | 99% | Sigma-Aldrich | $C_6H_4(NH_2)_2$ |
| Salicylic acid | ≥99.0% | SD fine | $C_7H_6O_3$ |
| 4-Nitrophthalonitrile | 99% | Sigma-Aldrich | $C_6H_4NO_2(CN)_2$ |
| Potassium carbonate | ≥99.0% | SD fine | $K_2CO_3$ |
| 1,8-Diazabicyclo [5.4.0]Undec-7-Ene | ≥99.0% (GC) | Sigma-Aldrich | DBU: $C_9H_{16}N_2$ |
| N-Pentanol | 99% | SD fine | $C_5H_{11}OH$ |
| Dimethylformamide | ≥98.5% | SD fine | DMF: $C_3H_7NO$ |
| Dimethylsulfoxide | ≥99.9% | SD fine | DMSO: $C_2H_6OS$ |
| Hydrochloric acid | 99% | SD fine | HCl |
| Sulfuric acid | 95.0–97.0% | SD fine | $H_2SO_4$ |
| Tetrabutylammonium perchlorate | ≥99.0% | Sigma-Aldrich | TBAP: $C_{16}H_{36}ClNO_4$ |
| Potassium bromide | 99% | Merck | KBr |
| Sodium hydroxide | 99% | SD fine | NaOH |
| Potassium ferrocyanide | ≥98.5% | SD fine | $K_4[Fe(CN)_6].3H_2O$ |
| Methanol | 99.8% | SD fine | $CH_3OH$ |
| Ethanol | 99% | SD fine | $C_2H_5OH$ |
| Acetone | ≥99.5% | SD fine | $CH_3COCH_3$ |
| N-Hexane | 99% | SD fine | $C_6H_{14}$ |
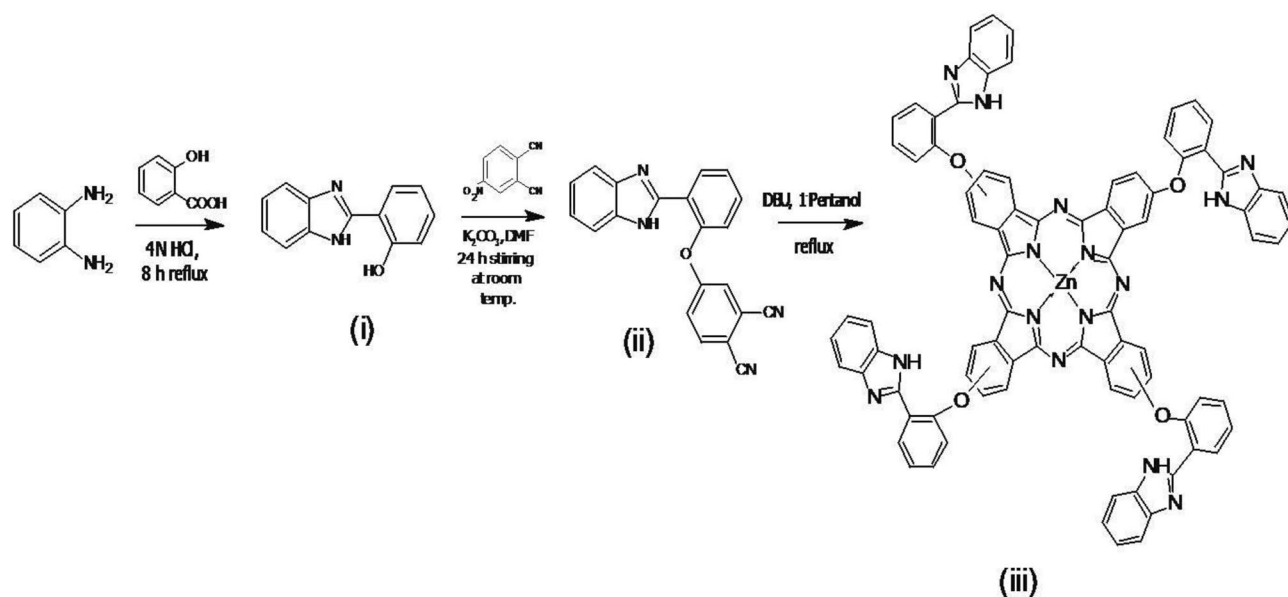
**Scheme 1** Synthetic route of ZnTBImPc

obtained was filtered and the precipitate washed successively with ethanol, acetone, and water.

Yield: 87%. Anal. for the compound **(iii)**, mol. wt 1439.81. $C_{85}H_{49}N_{16}O_5Zn$: Calc. (%) C, 70.84; H, 3.40; N, 15.55; O, 5.55; Zn: 4.51. Found (%): C, 70.35; H, 3.61; N, 15.82; Zn: 4.11. UV–VIS [DMSO, $\lambda_{max}$ (nm)]: 280, 350, 620, and 680. FTIR bands [KBr (pellet), $cm^{-1}$]: 740, 810, 910, 1090, 1152, 1208, 1247, 1312, 1428, 1522, 1535, 2950, 3025, and 3400. mass: 1438 ($M^{-2}$).

## 2.5 Characterization methods and Analyte preparation

Elemental analysis was performed with the Vario EL III CHNS elemental analyzer. The percentage of the metal content in the ZnTBImPc complex was determined by the gravimetric procedure. UV–Vis absorption spectrum was recorded using Ocean optics spectrometer with serial number: FLMSO 4808 in the region 300–800 nm with 0.1 mM ZnTBImPc complex in DMSO. FTIR spectra were collected using the KBr pellet sampling technique from FTIR Perkin Elmer Spectrum-Two spectrophotometer in the region 4000–500 $cm^{-1}$. Mass spectra were obtained from the 6100 series GC/MS instrument from Agilent technology. XRD pattern of the complex was recorded using Bruker D8 Advance X-ray diffraction machine using Cu Kα radiation. The thermal stability of the complex was monitored using STA6000 machine in the temperature range of 30 to 700 °C (heating rate of 10 °C $min^{-1}$) in the air atmosphere.

CHI6005E electrochemical analyzer was employed for electrochemical studies. The cell for electrochemical studies consisted of three electrode system. The GCE of surface area 0.0701 $cm^2$ was used for electropolymerization and subsequent sensing experiments with a saturated Ag/AgCl (3 M KCl) as reference and a platinum wire as counter electrode. The experiments related to electrochemistry were carried out in inert atmosphere by purging the $N_2$ gas for 20 min before each experiment.

The electrochemical cleaning of GCE was done by cycling of potential between − 0.2 and 1.0 V in 0.5 M $H_2SO_4$ at 50 mV $s^{-1}$ scan rate for 20 cycles which was then followed by cycling in the potential range of + 0.4 to − 1.8 V in 1 M KOH at a scan rate 50 mV $s^{-1}$ for 20 cycles. Then, the GCE was polished manually using polishing kit with 0.3 and 0.05 μm alumina powder alternatively on micro-cloth polishing pad and sonicated with alcohol and water twice for 5 min and washed with double-distilled $H_2O$ thoroughly and dried.

0.1 M ammonia stock solution was prepared by diluting with distilled water. Different volumes of 0.1 mM working standard $NH_3$ solution were added to electrochemical cell containing 10 mL 0.2 M di-sodium hydrogen phosphate/ sodium hydroxide buffer (pH 12.0) solution. The $NH_3$ concentration in the electrochemical cell after the addition of 5 μL of 0.1 mM ammonia working standard solution was 0.05 μM.

## 3 Results and discussion

The schematic route for the synthesis of ZnTBImPc is shown in Scheme 1. The first step involved the reaction between o-phenylenediamine and Salicylic acid to form

benzimidazole as shown in Scheme 2. The second step involves the synthesis of 4-[2-(1H-benzimidazol-2-yl) phenoxy] benzene-1, 2-dicarbonitrile ligand (**ii**), as shown in Scheme 1. The synthesis of **ii** is taken place by the nucleophilic substitution reaction between 2-(1H-benzimidazol-2-yl) phenol precursor (**i**) and nitrophthalonitrile.

Finally, targeted ZnTBImPc was synthesized by reacting phthalonitrile ligand (**ii**) with zinc salt and DBU in 1-pentanol by refluxing for 24 h. The obtained dark blue product was washed with methanol and subsequently with alkali/acid treatment. Precursor, ligand, and complex were obtained in good yield. The percent yield was calculated by dividing the experimental yield by the theoretical yield and multiplying the result by 100.

The final product ZnTBImPc is bluish green in color and amorphous in nature, and it is insoluble in aqueous solvents and soluble in non-aqueous solvents such as dimethyl sulfoxide (DMSO), dimethyl formamide (DMF), dimethyl amide (DMA), and also in conc. $H_2SO_4$.

## 3.1 UV–Visible spectrum

UV–Vis spectral characterization of 0.1 mM ZnTBImPc in DMSO was performed in the region 250–850 nm (Fig. S1). The ZnTBImPc complex showed peak at 320 nm (B-band) corresponding to $n \rightarrow \pi*$ transition and 685 nm (Q-band) corresponds to $\pi \rightarrow \pi*$ transition. The deep bluish green color of the synthesized compound is associated with the strong Q-band absorption peak observed in the visible region. The shoulder peak noticed at 630 nm may be ascribed to dimer and oligomeric complex species in

addition to vibronic fine structure of the phthalocyanine macrocycle [24, 25]. The B-band and Q-band peaks showed shift in the $\lambda_{max}$ compared to its parent MPc due to the extensive conjugation in ZnTBImPc molecule [25–27].

## 3.2 FTIR spectra

The FTIR spectra of the precursor (**i**), ligand (**ii**), and ZnTBImPc (**iii**) were carried out in 500 to 4000 cm$^{-1}$ range and are illustrated in Fig. 1. The precursor (**i**) displayed a peak at 1620 cm$^{-1}$ for C=N stretching. The peak at 2950 cm$^{-1}$ corresponds to aromatic –CH stretching, 1240 cm$^{-1}$ peak can be assigned to C–OH, and broad peak around 3200–3450 cm$^{-1}$
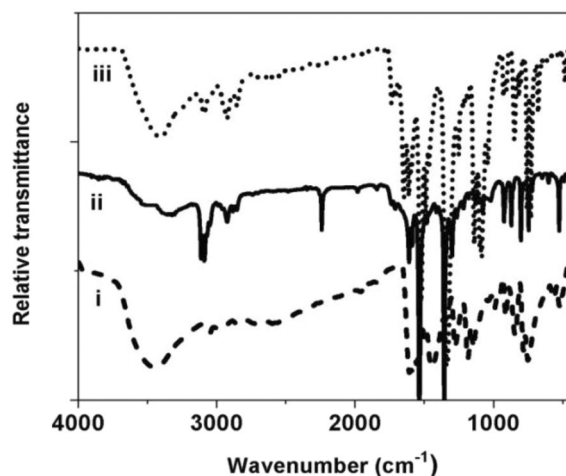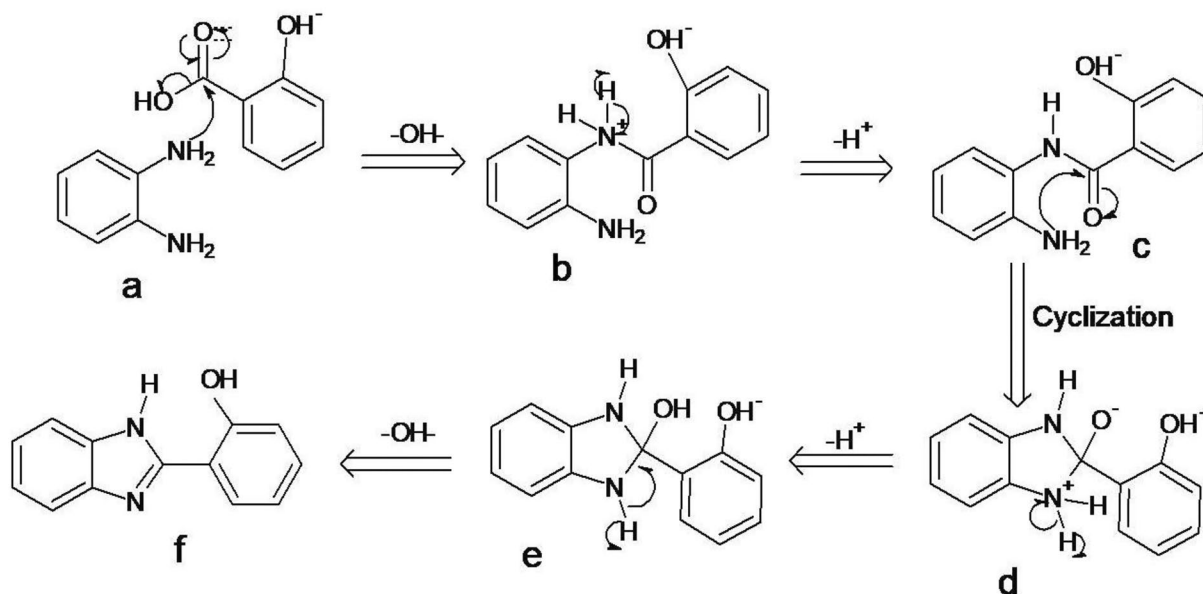


**Fig. 1** FTIR spectra of (i) precursor, (ii) ligand, and (iii) ZnTBImPc



**Scheme 2** Mechanism for the cyclization reaction between *O*-phenylenediamine and carboxylic group to form benzimidazole

corresponds to the –OH group. The ligand (**ii**) exhibited peaks similar to the precursor (i) with a supplementary peak at 2242 cm$^{-1}$ for the –CN group. The appearance of –CN band denotes the formation of phthalonitrile ligand (**ii**). The ZnTBImPc (**iii**) displayed characteristic bands at 742, 807, 910, 1091, and 1152 cm$^{-1}$ in the fingerprint region which are characteristic peaks of phthalocyanine skeleton vibrations [16, 21]. The nitrile peak at 2242 cm$^{-1}$ vanished in the spectrum of ZnTBImPc indicating quantitative conversion of phthalonitrile ligand to ZnTBImPc complex [26–29].

### 3.3 NMR-spectra

The purity of the phthalonitrile ligand (ii) was examined by $^1$H-NMR, and the spectrum is presented as Fig. S2. The chemical shift data obtained for various protons of phthalonitrile ligand (**ii**) are given in the synthetic part. The peak around 5.4 ppm can be designated to proton of amine and the peaks around 6.6 to 7.4 for aromatic protons.

### 3.4 Mass spectra

The mass spectra were used to confirm the formation of precursor (**i**), ligand (**ii**), and ZnTBImPc (**iii**) and the mass spectra are shown in Figs. S3, S4, and S5. The mass spectrum of synthesized precursor (**i**) yielded a peak at $m/z = 211$ (Fig. S3) equivalent to $M^{+1}$ molecular ion peak, and ligand (**ii**) displayed peak at $m/z = 334$ (Fig. S4) analogous to $M^{-2}$ molecular ion peak. The ZnTBImPc (**iii**) has a theoretical molecular mass of 1439.81, and the mass spectrum in Fig. S5 showed peaks at $m/z = 1438$, 1437, and 1435 ascribed to $M^{-1}$, $M^{-2}$ and $M^{-4}$ molecular ion peaks of ZnTBImPc.

### 3.5 X-ray diffraction studies

XRD profile was obtained for the synthesized substance to yield information on crystalline behavior. The XRD profile of ZnTBImPc was recorded in $2\theta$ angle 5°–80° range, Fig. S6. Exceptionally noisy and broader peaks were observed in the XRD profile of the ZnTBImPc (**iii**) complex which may be due to the amorphous nature of the benzimidazole phthalocyanine. The XRD pattern of complex (**iii**) showed diffusive peaks at $2\theta = 20.58°$, 29.12°, 45.22°, 47.27°, and 62.39°.

### 3.6 Thermogravimetric studies

TGA was performed to acquire information about the thermal stability and decomposition behavior of the ZnTBImPc at elevated temperatures. Thermogravimetric curve for ZnTBImPc is shown in Fig. S7. The nature of TGA profile demonstrates that the complex is stable up to 380 °C and degrades at high temperatures. The loss

of moisture was observed in the range 100–130 °C. The weight loss occurred around 380–450 °C corresponds to the degradation and decomposition of the organic phthalocyanine moiety. The Pc complex did not show a sharp melting point but decompose at higher temperatures as reported for other phthalocyanines in the literature [16, 23]. The end product observed from the stable horizontal line after 500 °C in the oxidizing atmosphere was found to be ZnO. The ZnTBImPc complex displayed higher decomposition temperature (charring temperature) compared to the parent as well as other Pc complexes [16] as a result of higher conjugation and better interaction and bonding in ZnTBImPc.

### 3.7 Cyclic voltammetric studies

#### 3.7.1 Solution CV

voltammetric studies convey information related to the redox behavior of the compounds. The cyclic voltammograms of 0.1 mM synthesized Pc in DMSO along with 0.1 M tetrabutyl ammonium perchlorate (TBAP) were recorded in the potential window of 1.0 to −1.0 V at a scan rate of 50 mV s$^{-1}$. The ZnTBImPc complex exhibited two pairs of redox peaks as shown in Fig. 2**.** The redox peak potentials at −0.72 and −0.420 V with peak-to-peak potential separation ($\Delta E$) of 300 mV were designated for the redox property of Pc macrocycle (Pc$^{-2}$/Pc$^{-3}$) and other redox couple with peak potentials at −0.02 and +0.248 V ($\Delta E = 268$ mV) can be ascribed to (Pc$^{-2}$/Pc$^{-1}$) [17]. Redox peaks for Zn metal ion were not noticed as Zn ion in phthalocyanine core is electrochemically inactive [19].
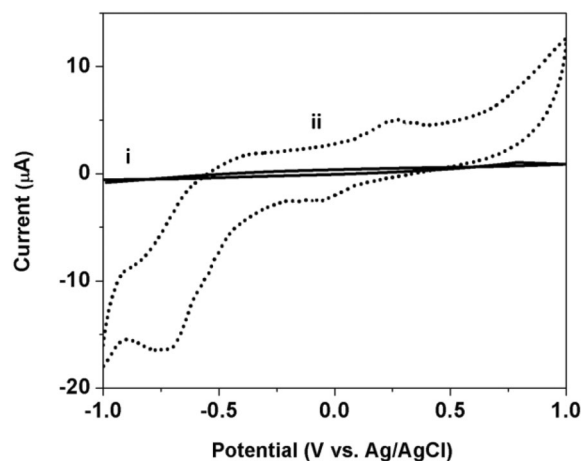


**Fig. 2** CV of bare GCE (i) and with (ii) ZnTBImPc complex in DMSO with 0.1 M TBAP under the current of $N_2$ gas at 50 mV s$^{-1}$

### 3.7.2 Electropolymerization

Cyclic voltammetry was performed to polymerize ZnT-BImPc on the glassy carbon electrode (GCE) using 1 mM ZnTBImPc in DMSO with 0.1 M TBAP. The potential was swept between $-1.2$ to $+1.1$ V at 50 mV s$^{-1}$. The resulting CVs for the polymerization of ZnTBImPc on GCE and CNP (5 μL of 1 mg/mL CNP in IPA was coated on GCE) coated GCE are shown in Fig. 3. The gradual increase in the background and peak currents for the successive CVs inferred that the additional monomer is attached to the oligomeric molecule during each potential cycle on the electrode surface and the polymeric film deposits on the GCE. Further, a slight potential shift was observed for the subsequent cycles because of the exposure of new polymeric surface during each potential scan. The electropolymerized film obtained after 50 cycles on GCE and CNP-coated GCE was rinsed with DMSO, ethanol, and dried. The polymeric electrodes were characterized by cyclic voltammetry in DMSO containing 0.1 M TBAP, and peaks similar to Pc in solution were noticed revealing the deposition of benzimidazole Pc polymeric film on the electrode surface.

### 3.7.3 Morphological investigation

Field emission scanning electron microscopy (FESEM) images were recorded to understand the morphology of the polymeric phthalocyanine on the electrode surface. SEM image of polymeric Pc in Fig. 4 exhibits an elongated morphology and characteristic of the molecules self-assembled through supramolecular aggregation. The polymer complex has dimensions of roughly about 10 μm length with 200 nm width.
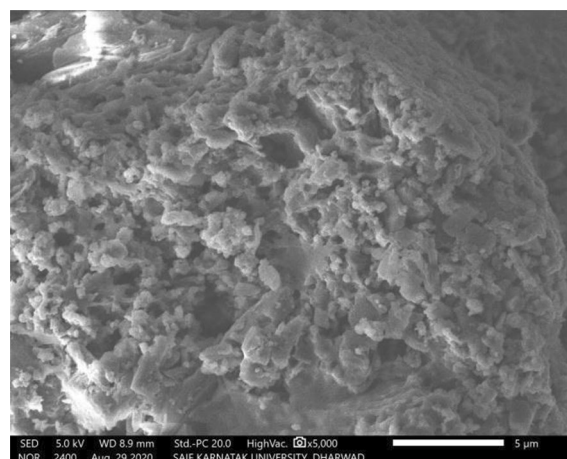


**Fig. 4** FESEM image of the poly(ZnTBImPc)-modified surface

### 3.7.4 Charge transfer studies

Cyclic voltammetry experiments were also conducted to study the charge transfer kinetics of the electrodes in 0.1 mM $[Fe(CN)_6]^{-3/-4}$ redox probe. Figure 5 shows the CVs for $[Fe(CN)_6]^{-3/-4}$ on bare GCE, GCE/poly(ZnTBImPc), and GCE/CNP-poly(ZnTBImPc) in di-sodium hydrogen phosphate/sodium hydroxide buffer of pH 12.0 at 50 mV s$^{-1}$ scan rate. The separation between the anodic peak to cathodic peak is slightly higher for GCE/poly(ZnTBImPc) compared to bare GCE whereas GCE/CNP-poly(ZnTBImPc) demonstrated peak separation similar to that of bare GCE. Further, the redox peak currents were highest for the polymeric Pc-CNP composite electrode than bare GCE. The slower electron exchange kinetics noticed at the poly(ZnTBImPc) can be attributed to the thickness as well as lesser conductivity
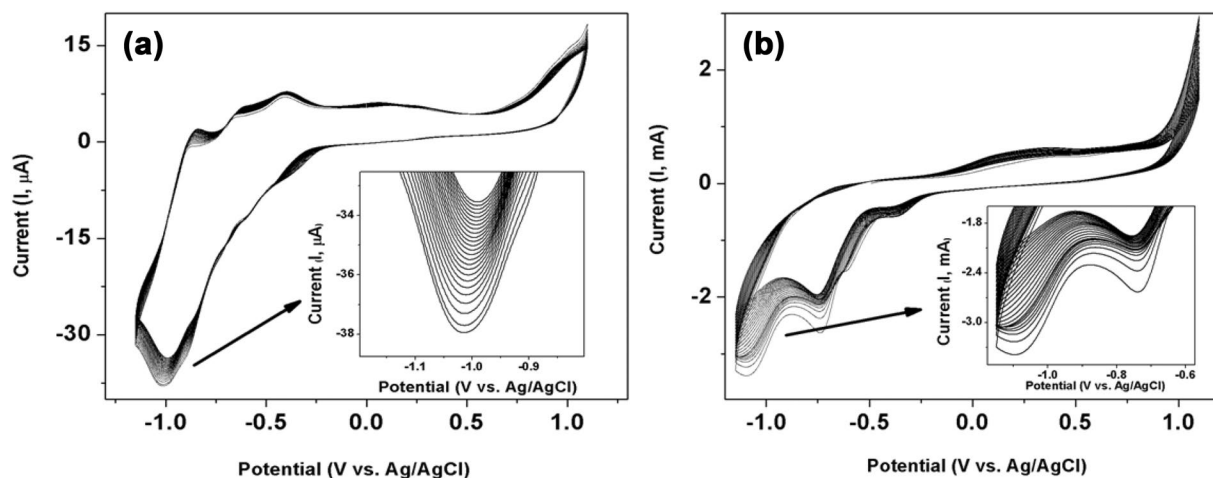


**Fig. 3** Cyclic voltammograms for the electropolymerization of 1 mM ZnTBImPc in DMSO at **A** GCE and **B** GCE/CNP at 50 mV s$^{-1}$ in N$_2$ atmosphere. Inset, magnified portion of CV during polymerization
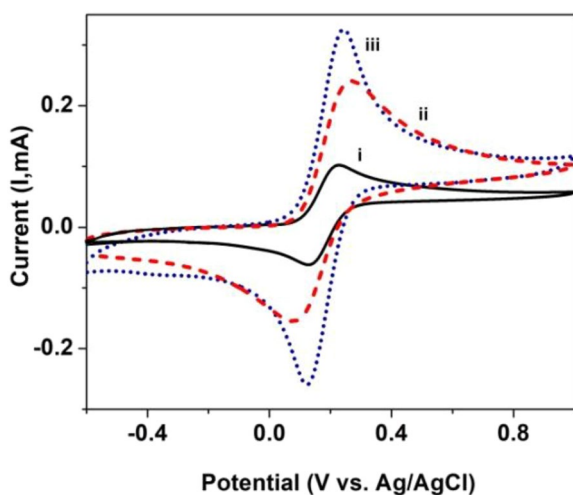
**Fig. 5** CV profile for $[Fe(CN)_6]^{-3/-4}$ (0.1 mM) at (i) Bare GCE, (ii) GCE/poly(ZnTBImPc), and (iii) GCE/CNP-poly(ZnTBImPc) electrode in buffer (pH 12.0)

of polymeric layer, which slightly behaves as a barrier for the electron transfer resulting in slow interfacial electron transfer. The faster and quick electron exchange kinetics for $[Fe(CN)_6]^{-3/-4}$ on hybrid GCE/CNP-poly(ZnTBImPc) compared to polymeric Pc film is the result of expanded surface area and increased conductivity provided by CNP to the hybrid system. The better charge transfer kinetics is also reported for the Pc-modified hybrid electrodes in the literature compared to bare GCE [20, 29–32].

# 4 Electrochemical detection of ammonia

The electropolymerized film on the GCE was employed for the sensing of ammonia in inert atmosphere. In order to understand the influence of pH on ammonia electro-oxidation, experiments were carried out in different pH solutions (pH 6, 8, 10, and 12). As can be noticed in Fig. S9, the ammonia oxidation current increased with pH value. This is ascribed to the increasing availability of $OH^-$ ions which results in the enhancement of peak current at higher pH solutions. However, the peak potential was unaltered. Hence, di-sodium hydrogen phosphate/sodium hydroxide buffer (pH 12.0) solution was used as optimum electrolyte in the detection of ammonia.

Figure S10 shows the CVs of bare GCE and polymeric film electrodes for the electrocatalytic oxidation of ammonia in buffer (pH 12.0) under $N_2$ atmosphere. The catalytic current was negligible at bare electrode for the oxidation of 0.1 μM ammonia whereas the polymeric electrodes displayed larger current response at lesser overpotential. The significantly remarkable current response was noticed for hybrid composite electrode compared to polymerized film

of Pc electrode. The larger current response as well as lower overpotential for $NH_3$ oxidation at the composite electrode may be accounted for the larger surface area and conductivity of CNP derived composite.

## 4.1 Cyclic voltammetric sensing of ammonia

The catalytic oxidation of ammonia at the polymeric electrodes motivated to study the current response for different concentrations of ammonia. The detection of ammonia was monitored by cyclic voltammetry using poly(ZnTBImPc) at 50 mV/s in buffer (pH 12.0) under $N_2$ atmosphere in the potential range of 0.6 to 1.2 V as shown in Fig. 6A. CVs displayed increase in current response with gradual increase in the concentration of $NH_3$. Graph of peak current ($i_p$) vs concentration of ammonia at 1.1 V exhibited linear response in 0.1 to 1 μM concentration range with straight line characteristics represented by $y = 16.630x + 2.3713$ ($R^2 = 0.9993$) with LOD = 33 nM and sensitivity value of 237.2325 μA $μM^{-1}$ $cm^{-2}$ for GCE/poly-ZnTBImPc.

Cyclic voltammograms for $NH_3$ oxidation in buffer (pH 12.0) at CNP-poly(ZnTBImPc) electrode was also recorded for various concentrations of ammonia (0.1 to 1 μM), Fig. 6B. The anodic current increased in the region of 0.6 to 1.2 V with increase in the concentration of ammonia which can be accounted for electrocatalytic ammonia oxidation at the composite electrode. The increase in oxidation current for ammonia was observed at lesser overpotential on composite hybrid electrode compared to bare GCE and polymeric Pc film electrode. The enhanced current with lesser overpotential for ammonia oxidation displayed by CNP-poly(ZnTBImPc) clearly indicates the catalytic nature and synergic effect of the composite electrode in the oxidation of ammonia. In addition, the better activity is accounted for the presence of CNP which provides more surface area, conductivity, and catalytic sites to the composite.

The graph of anodic current vs. concentration of ammonia at 1.1 V produced linear plot in the range 0.1 to 1 μM at GCE/CNP-poly(ZnTBImPc) with straight line characteristics; $y = 35.1042x + 1.5533$, ($R^2 = 0.9976$) with LOD = 20 nM and sensitivity of 500.7731 mA $μM^{-1}$ $cm^{-2}$. The GCE/CNP-poly(ZnTBImPc) electrode exhibited better sensitivity and LOD for the detection of $NH_3$ compared to GCE/poly(ZnTBImPc).

## 4.2 Effect of scan rate

CVs were recorded for 0.2 μM ammonia in buffer (pH 12.0) at different scan rates, i.e., 25 to 700 mV $s^{-1}$ on composite electrode as in Fig. S11A. The increase in scan rate resulted in the increase in oxidation peak current due to the oxidation of ammonia. The plot of current response vs square root of scan rate at 1.1 V is as shown in Fig. S11B which exhibited
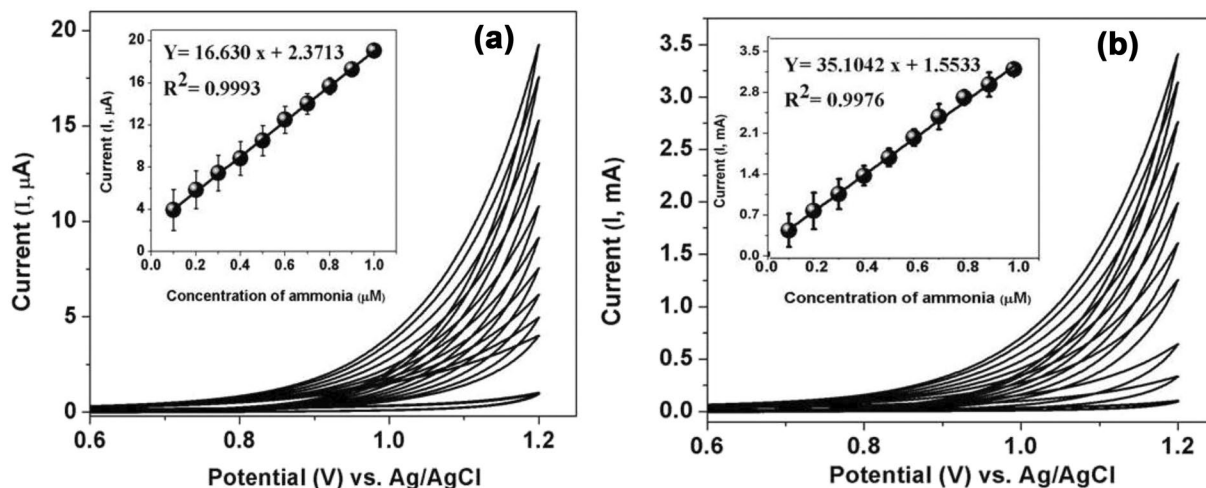
**Fig. 6** Cyclic voltammograms at **A** GCE/poly(ZnTBImPc) and **B** GCE/CNP-poly(ZnTBImPc) with different concentrations of ammonia (0.1 to 1 μM) in buffer (pH 12.0). Inset, plot of anodic peak current vs. ammonia concentration at 1.1 V

linear plot confirming diffusion-controlled mass transfer process in the oxidation of $NH_3$ [18, 21].

The diffusion coefficient ($D$) for the oxidation reaction of ammonia at the GCE/CNP-poly(ZnTBImPc) was calculated with the help of Randles–Sevcik equation (Eq. 1) [33].

$$I_p = 2.69 \times 10^5 v^{1/2} n^{3/2} C A D^{1/2},\qquad(1)$$

where $I_p$ is the peak current in $A$, n is the number of electrons that take part in ammonia oxidation reaction, i.e., $n = 3$, $v$ is scan rate in mV/s, $C$ is ammonia concentration (0.2 μM), and $A$ is the surface area of electrode. The $D$ value was found to be $2.31 \times 10^{-5}$ cm$^2$ s$^{-1}$. The $D$ value indicates the ability of ammonia to diffuse across a unit area in 1 s under the influence of a potential gradient of one unit. In general, higher $D$ value accounts for the faster diffusion of the analytic species across the electrode. The observed $D$ value is almost agreeing with the D value reported in the literature for ammonia oxidation [34].

## 4.3 Amperometric detection of ammonia

Chronoamperometric method is highly sensitive method for the detection of small amount of analyte species. Amperometric sensing of ammonia was carried out at GCE/poly(ZnTBImPc) and GCE/CNP-poly(ZnTBImPc) in buffer (pH 12.0) with an applied potential of 1.1 V under stirring condition. The current–time response was monitored with the repetitive addition of ammonia. The step current obtained for the successive addition of 0.05 μM ammonia in buffer (pH 12.0) at the bare as well as modified electrodes with the time interval of 50 s is as shown in Fig. 7A. The amperometric step current response was quick for the addition of ammonia at the

modified electrodes. Further, the step current increased linearly with the increase in ammonia concentration. The corresponding graph of step current vs concentration, Fig. 7B, exhibited linear response for ammonia oxidation in the 0.05 to 0.5 μM concentration range with $R^2 = 0.9821$ and 0.9973 for the poly(ZnTBImPc) and CNP-poly(ZnTBImPc) electrodes, respectively. The $R^2$ value represents the better linear relationship between step current and concentration of $NH_3$ at the Pc and hybrid-modified GCE. The linear plots in Fig. 7B exhibited straight line characteristics represented by $y = 32.17x + 0.7766$ and $y = 48.73x + 0.992$ for the GCE/poly(ZnTBImPc) and GCE/CNP-poly(ZnTBImPc), respectively. The LOD was 20 nM at GCE/poly(ZnTBImPc) with sensitivity value 458.91 μAμM$^{-1}$ cm$^{-2}$ and GCE/CNP-poly(ZnTBImPc) displayed LOD value 10 nM with a superior sensitivity value of 695.14 μAμM$^{-1}$ cm$^{-2}$. In addition, the composite electrode demonstrated better catalytic activity for $NH_3$ oxidation in comparison to the electrode materials reported in the literature and summarized in Table 2.

## 4.4 Tafel plot

Figure 8 shows the Tafel plot for the ammonia oxidation which was extracted from Fig. 6B at various concentrations. The plot in Fig. 8 presents a slope value of about 40 mV which is in fair agreement with the scan rate-dependent data (Fig. S11). In addition, there was no significant change in the slope value with varying ammonia concentration. This slope value informs that the ammonia oxidation involved the adsorption effects and/or subsequent intermediate chemical reaction at the modified electrode surface [34–36].
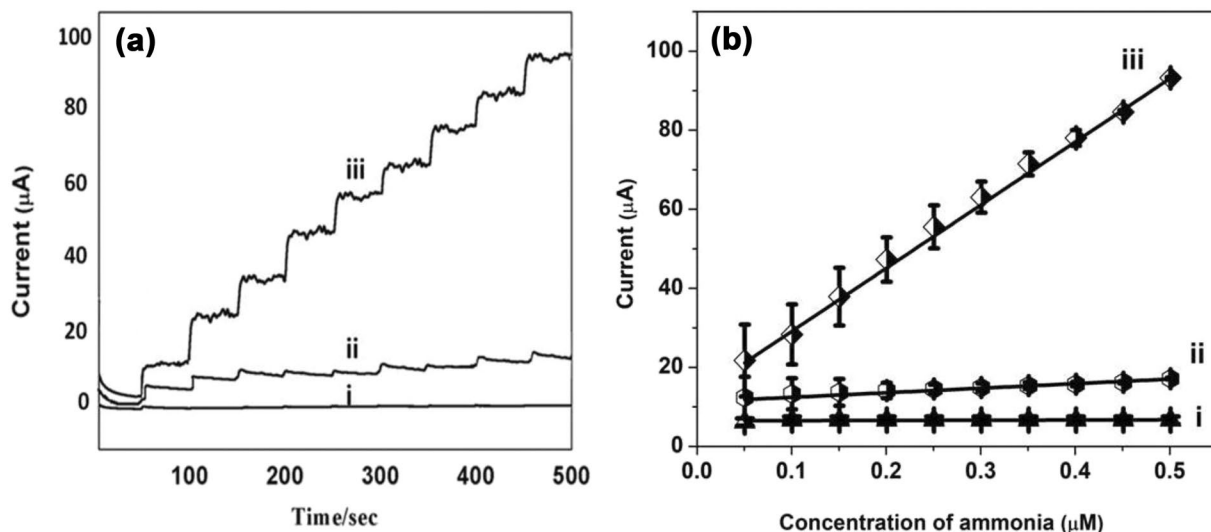
**Fig. 7 A** Chronoamperometric curves for the successive addition of ammonia (0.05 to 0.5 μM) in buffer (pH 12.0) at (i) bare GCE, (ii) GCE/poly(ZnTBImPc), and (iii) GCE/CNP-poly(ZnTBImPc) at 1.1 V under stirring condition. **B** Plot of amperometric current vs. conc. of ammonia on different electrodes

**Table. 2** Comparison of the GCE/CNP-poly(ZnTBImPc) with different electrodes in the literature for the sensing of ammonia

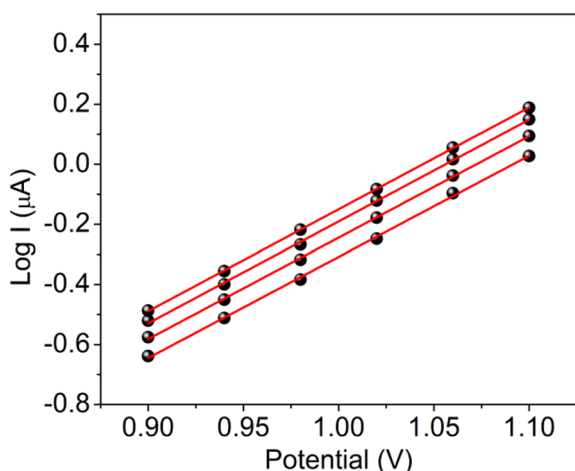| Electrode material | Method | Dynamic range | LOD | Sensitivity | References |
|---|---|---|---|---|---|
| ZnO nanopencils | CV | 0.5 to 5 mM | 5.0 μM | 26.5822 μA cm$^{-2}$ mM$^{-1}$ | [37] |
| Polyurethane acrylate | CV | 0.05 to 0.5 mM | 0.018 M | 8.5254 μA cm$^{-2}$ mM$^{-1}$ | [38] |
| β-Fe$_2$O$_3$ nanoparticles | CV | 77 μM to 7.7 M | 21.8 M | 0.5305 μA cm$^{-2}$ mM$^{-1}$ | [39] |
| CuO-codoped ZnO nanorods | CV | – | 8.9 M | 1.549 μA cm$^{-2}$ mM$^{-1}$ | [40] |
| poly(ZnTBImPc) | CV | 0.1 to 1 μM | 0.03 μM | 237.23 μA cm$^{-2}$ μM$^{-1}$ | This work |
|  | CA | 0.05 to 0.5 μM | 0.02 μM | 458.91 μA cm$^{-2}$ μM$^{-1}$ |  |
| CNP-poly(ZnTBImPc) | CV | 0.05 to 1 μM | 0.02 μM | 500.77 mA cm$^{-2}$ μM$^{-1}$ |  |
|  | CA | 0.05 to 0.5 μM | 0.01 μM | 695.14 μA cm$^{-2}$ μM$^{-1}$ |  |



**Fig. 8** Tafel plot for the different concentrations of ammonia where the data extracted from Fig. 6B

### 4.5 RDE measurements

The rate of a reaction at an electrode surface is dependent on mass transport and kinetics. Rotating disk electrode has been employed to yield the mass transport parameters (e.g., diffusion coefficient) and the kinetic parameters (i.e., standard rate constant, $k^0$) using the Levich equation [40]. Potential sweep reversals in RDE system are quite different from the cyclic voltammetry as the products of the potential sweep are continually swept away from the electrode in case of RDE. A reversal sweep produces a similar *I–V* curve which closely matches the forward scan except the capacitive charging current. The peak current in the cyclic voltammogram for a RDE is a plateau-like region, governed by the Levich equation [41–44]. The limiting current incase of RDE is typically much higher than the peak current of a stationary electrode, revealing that the mass transport of reactants is actively stimulated by the rotating disk,

and not just by diffusion as is the case of stationary electrode. The LSV measurements have been carried out under different rotation speeds and plotted the Koutecky–Levich plot.

The RDE experiment for the modified electrode was performed in buffer (pH 12.0) at various rotational speeds. Linear sweep voltammograms (LSV) for 0.1 μM ammonia in buffer (pH 12.0) were recorded at 25 °C with various rotation rates (200 to 1000 rpm) at a scan rate of 5 mV s$^{-1}$ and are presented in Fig. 9a. The blank electrolyte solution displayed shift in the oxidation current to lesser value with increase in the electrode rotational speed compared to the static condition (0 rpm). The reproducibility of the peak current density with each angular velocity was confirmed by several measurements made under the same conditions. The oxidation of ammonia resulted in the current difference between the maxima and minima of peak current, shown in Fig. 9a. The changes in ammonia oxidation peak current can be related to mass transfer effects as validated in the scan rate-dependent analysis, Fig. S11.

The corresponding K–L plot is shown in Fig. 9b. The graph of 1/J vs 1/ω$^{1/2}$ was plotted at different potentials of 1.12 V, 1.14 V, 1.16 V, 1.18 V, and 1.2 V. The number of electrons transferred during the electrochemical oxidation of ammonia was calculated with the help of K–L plot and is found to be $n = 2.56$. This value is close to $n = 3$ and matches with the predicted electrochemical oxidation of ammonia as in Eq. 2.

$$NH_3(aq) \rightarrow N_2 + 3H_2 + 3e^-. \tag{2}$$
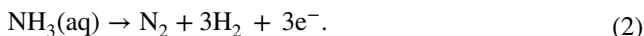
## 4.6 Interference studies and real sample analysis

The selectivity and specificity of the fabricated *GCE/CNP-poly(ZnTBImPc)* sensor was investigated for the sensing

of ammonia in the presence of biological electroactive species and inorganic compounds. Figure 10 displays the amperometric response for (a) 0.05 μM ammonia and the successive addition of 1 mM (b) glucose, (c) ascorbic acid, (e) hydroquinone, and the inorganic salts namely (d) NaNO$_2$, (f) KCl, and (g) KNO$_3$ at periodic interval of 50 s into buffer (pH 12.0) at a fixed potential of 1.1 V on GCE/CNP-poly(ZnTBImPc) electrode. The step current response was noticed for the addition 0.05 μM ammonia, but there was no significant change in the amperometric response on adding even excess amount of different co-existing compounds. However, the addition of NH$_3$ into the buffer (pH 12.0) solution in the presence of higher amounts of various
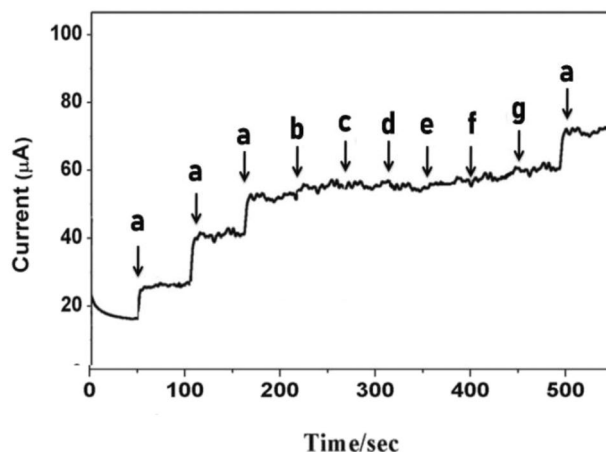


**Fig. 10** Amperometric *I–T* response for **a** 0.05 μM ammonia and 1 mM of **b** glucose, **c** ascorbic acid, **d** NaNO$_2$, **e** hydroquinone, **f** KCl, and **g** KNO$_3$ in di-sodium hydrogen phosphate/sodium hydroxide buffer (pH 12.0) at GCE/CNP-poly(ZnTBImPc)
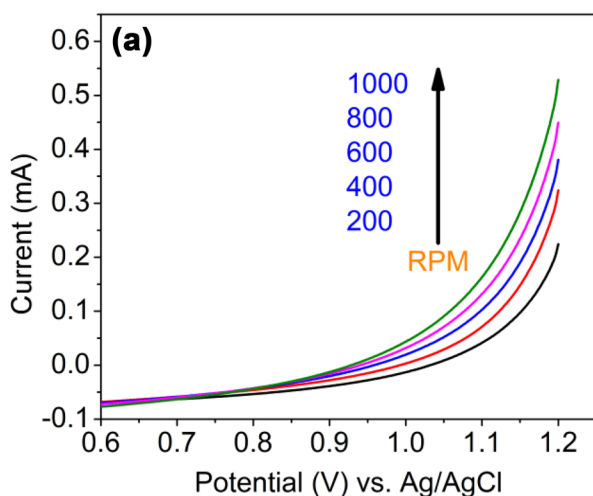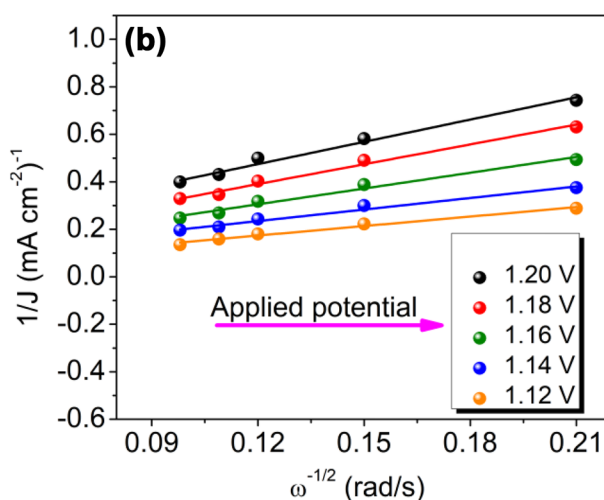


**Fig. 9** **a** LSV for modified electrode at the rotation speed of 200 to 1000 rpm on rotating GC disk electrode in 0.1 μM ammonia solution in buffer (pH 12.0) and scan rate 5 mVs$^{-1}$, **b** the K–L plot of modified electrode, obtained based on the LSV data of **a**. All potentials are measured using Ag/AgCl as a reference electrode

interfering species displayed an enhancement in the step current. This indicates that the CNP-poly(ZnTBImPc) electrode has remarkable selective response for ammonia analyte even in the presence of co-existing bio-electroactive species and inorganic salts.

The CNP-poly(ZnTBImPc) sensor was utilized for ammonia detection in real sample. The agricultural waste water from nearby place (Kampli, Ballari, India) was taken for the detection of ammonia at GCE/CNP-poly(ZnTBImPc). 1.0 mL filtered agriculture water sample was injected into the buffer (pH 12.0) for the detection and determination of $NH_3$. The current response was negligible inferring that the ammonia content in agricultural water sample is either negligible or less than the linear range of the proposed sensor. The agricultural waste water sample was then spiked with known amount of ammonia, and the recovery values at the modified electrode were close to the theoretical values which revealed that the matrices in sample do not interfere during the detection of ammonia at CNP-poly(ZnTBImPc), and recovery values are summarized in Table 3.

In order to understand the interaction of the ZnTBImPc with the ammonia analyte, UV–Vis spectrometry in DMSO was carried out (Fig. S12). The absorption spectra of 0.1 mM ZnTBImPc in DMSO demonstrated narrow Q-band, whereas the addition of 200 nM ammonia analyte leads to the shifting of Q-band towards the longer wavelength region indicating strong interaction between the Pc complex and $NH_3$.

### 4.7 Stability, reproducibility, and repeatability of modified electrodes

In order to commercialize the fabricated sensor, reproducibility and repeatability of the developed sensor for the oxidation of ammonia were investigated. To assess the reproducibility in the fabrication procedure of the composite hybrid electrode, 0.1 μM ammonia oxidation was carried out on five different fabricated composite electrodes prepared under same conditions. The relative standard deviation for the oxidation peak current at different modified electrodes was established to be less than 2.1%. Further, the RSD value was less than 1.8% for four replicate amperometric measurements of ammonia oxidation at hybrid electrode of ZnTBImPc. The stability of the GCE/CNP-poly(ZnTBImPc) was monitored by comparing the amperometric response of the freshly prepared electrode and after storing the electrode in

vacuum desiccator for 7 days. The amperometric current response of the designed CNP-poly-ZnTBImPc stored for seven days was in good agreement with that of the response of the fresh electrode which suggests that the designed GCE/CNP-poly(ZnTBImPc) is stable for more than a week if stored properly in inert conditions. In addition, the electrochemical stability of the fabricated sensor was assessed by cycling the potential in the range 0 to 1.2 V repetitively for 100 cycles in buffer (pH 12.0) electrolyte, and only 2.6% loss in the peak current was observed for the polymeric film electrode after 100 cycles which demonstrates the good electrochemical stability of the designed hybrid electrode. The stability can be attributed to strong interaction between the π-electrons of Pc polymer with the electrode surface.

## 5 Conclusion

Novel N4 macrocyclic complex, tetrabenzimidazole-substituted zinc phthalocyanine (ZnTBImPc) was synthesized and characterized with different physico-chemical techniques. The spectral analysis indicated that the synthesized complex is pure in nature. The synthesized molecule is electroactive in nature and was electropolymerized on the GCE. The electrocatalytic activity of the poly(ZnTBImPc) for the ammonia oxidation was compared with the composite hybrid-modified electrode designed by electropolymerizing ZnTBImPc on CNP-coated GCE. The fabricated polymeric film electrode showed linear response for ammonia oxidation in the range of 0.1 to 1.0 μM with LOD of 0.03 μM and sensitivity of 237.25 μA μM$^{-1}$ cm$^{-2}$ whereas the composite hybrid electrode of poly(ZnTBImPc) and carbon nanoparticle (CNP) showed a better sensitivity of 500.77 μA μM$^{-1}$ cm$^{-2}$ and linear range of 0.05 to 1 μM with LOD of 0.02 μM. The amperometric sensing of ammonia showed linear behavior in 0.05 to 0.5 μM concentration range with 0.01 μM of LOD and 695.14 μA μM$^{-1}$ cm$^{-2}$ sensitivity at the fabricated composite electrode. The RDE experiment revealed that the number of electrons involved in the ammonia oxidation is nearly 3. The polymeric composite electrode was subjected to the interference studies to evaluate the selectivity of the fabricated electrode and found that the co-existing molecules do not show interference during the detection of ammonia. The composite hybrid electrode of CNP-poly(ZnTBImPc) displayed better activity in terms of current response and

**Table 3** Analytical data obtained for the agricultural waste water sample analysis at CNP-poly(ZnTBImPc)

| Sample | Spiked (nM) | Detected (nM) | Recovery (%) | RSD (%) |
|---|---|---|---|---|
| Agricultural wastewater sample | 200 | 203 | 101.5 | 2.60 |
| | 400 | 405 | 101.2 | 2.13 |
| | 600 | 604 | 100.7 | 1.46 |

sensitivity which may be accounted for the presence of CNP as it enhances the conductivity as well as surface area of composite. The intercalation of CNP with the conjugated polymeric phthalocyanine provides a better platform for the sensing of ammonia and also may be for other analytes due to the improved conductivity and surface area.

# References

1. Sizun T, Bouvet M, Suisse JM (2012) Humidity effect on ammonia sensing properties of substituted and unsubstituted cobalt phthalocyanines. Talanta 97:318–324

2. Volkow ND, Gur RC, Wang GJ et al (1998) Association between decline in brain dopamine activity with age and cognitive and motor impairment in healthy individuals. Am J Psychiatry 155:344–349

3. Malenka RC, Nestler EJ, Hyman SE, Sydor A, Brown RY (2009) Molecular neuropharmacology: a foundation for clinical neuroscience, 2nd edn, vol 147–48: 366–367, 375–376. McGraw-Hill Medical, New York

4. Rahman MM, Balkhoyor HB, Asiri AM, Marwasni HM (2016) A gold electrode modified with silver oxide nanoparticle decorated carbon nanotubes for electrochemical sensing of dissolved ammonia. Microchim Acta 183:1677–1685

5. Berridge KC, Robinson TE, Aldridge JW (2009) Dissecting components of reward: "liking", "wanting", and learning. Curr Opin Pharmacol 9:65–73

6. Ding H, Cai Y, Chen J et al (2019) Cryodesiccation-driven crystallization preparation approach for zinc(II)-phthalocyanine nanodots in cancer photodynamic therapy and photoacoustic imaging. Microchim Acta 186:2–9

7. Hahn U, Engmann S, Oelsner C et al (2010) Immobilizing water-soluble dendritic electron donors and electron acceptors—phthalocyanines and perylenediimides—onto single wall carbon nanotubes. J Am Chem Soc 132:6392–6401

8. Denisha G, Nolwazi N, Werner E (2020) Recent advances in phthalocyanines for chemical sensor, non-linear optics (NLO) and energy storage applications. Coord Chem Rev 420:213359

9. Imadadulla M, David O, Manjunatha N, Lokesh KS, Tebello N (2019) Investigation of novel substituted zinc and aluminium phthalocyanines for photodynamic therapy of epithelial breast cancer. Dyes Pigments 170:107592

10. Keshavananda Prabhu CP, Manjunatha N, Muthumuni M, Tebello N, Lokesh KS (2021) Symmetrically substituted Zn and Al phthalocyanines and polymers for photodynamic therapy application. Front Chem 9:331

11. Nilotpal B, Biswajit N, Abhijit G, Gopal D (2019) A benzimidazole-based non-symmetrical tripodal receptor for the ratiometric fluorescence sensing of fluoride ions and solid state recognition of sulfate ions. New J Chem 43:16497

12. Sahar Z-A, Maryam SM, Omid A, Masoud S-N (2020) Green synthesis of dysprosium stannate nanoparticles using *Ficus carica* extract as photocatalyst for the degradation of organic pollutants under visible irradiation. Ceram Int 46:6095–6107

13. Mugadza T, Nyokong T (2010) Synthesis, characterization and the electrocatalytic behaviour of nickel (II) tetraamino-phthalocyanine chemically linked to single walled carbon nanotubes. Electrochim Acta 55:6049–6057

14. Moraes FC, Golinelli DLC, Mascaro LH, MacHado SAS (2010) Determination of epinephrine in urine using multi-walled carbon nanotube modified with cobalt phthalocyanine in a paraffin composite electrode. Sens Actuators B 148:492–497

15. Zhang T, Mubeen S, Myung NV, Deshusses MA (2008) Recent progress in carbonnanotube-based gas sensors. Nanotechnology 19:2001

16. Bondavalli P, Legagneux P, Pribat D (2009) Carbon nanotubes based transistors as gas sensors: state of the art and critical review. Sens Actuators B 140:304–318

17. Keshavananda Prabhu CP, Nemakal M, Aralekallu S et al (2019) A comparative study of carboxylic acid and benzimidazole phthalocyanines and their surface modification for dopamine sensing. J Electroanal Chem 847:113262

18. Palanna M, Mohammed I, Aralekallu S, Nemakal M, Sannegowda LK (2020) Simultaneous detection of paracetamol and 4-aminophenol at nanomolar levels using biocompatible cysteine-substituted phthalocyanine. New J Chem 44:1294–1306

19. Verma AL, Saxena S, Saini GSS et al (2011) Hydrogen peroxide vapor sensor using metal-phthalocyanine functionalized carbon nanotubes. Thin Solid Films 519:8144–8148

20. Özgül G, Taştemel A, Özkaya AR, Bulut M (2015) Synthesis, characterization and comparative electrochemistry of beta and alpha tetra-[4-oxy-3-methoxybenzoic acid]-substituted Zn(II), Co(II) and Cu(II) phthalocyanines. Polyhedron 85:181–189

21. Hu YF, Zhang ZH, Bin ZH et al (2012) Sensitive and selective imprinted electrochemical sensor for p-nitrophenol based on ZnO nanoparticles/carbon nanotubes doped chitosan film. Thin Solid Films 520:5314–5321

22. Keshavananda Prabhu CP, Manjunatha N, Shambhulinga A et al (2019) Synthesis and characterization of novel imine substituted phthalocyanine for sensing of L-cysteine. J Electroanal Chem 834:130–137

23. Fashedemi OO, Ozoemena KI (2011) A facile approach to the synthesis of hydrophobic iron tetrasulfophthalocyanine (FeTSPc) nano-aggregates on multi-walled carbon nanotubes: a potential electrocatalyst for the detection of dopamine. Sens Actuators B 160:7–14

24. Aralekallu S, Mohammed I, Manjunatha N et al (2019) Synthesis of novel azo group substituted polymeric phthalocyanine for amperometric sensing of nitrite. Sens. Actuators B 282:417–425

25. Gaudillat P, Jurin F, Lakard B et al (2014) From the solution processing of hydrophilic molecules to polymer-phthalocyanine hybrid materials for ammonia sensing in high humidity atmospheres. Sensors (Switzerland) 14:13476–13495

26. Sajjan VA, Aralekallu S, Nemakal M, Palanna M, Prabhu CPK, Sannegowda LK (2020) Nanomolar detection of lead using electrochemical methods based on a novel phthalocyanine. Inorg Chim Acta 506:9564

27. Nyokong T, Vilakazi S (2003) Phthalocyanines and related complexes as electrocatalysts for the detection of nitric oxide. Talanta 61:27–35

28. Aralekallu S, Sajjan VA, Palanna M et al (2020) Ni foam-supported azo linkage cobalt phthalocyanine as an efficient electrocatalyst for oxygen evolution reaction. J Power Sources 449:227516

29. Gao F, Cai X, Wang X et al (2013) Highly sensitive and selective detection of dopamine in the presence of ascorbic acid at graphene oxide modified electrode. Sens. Actuators B 186:380–387

30. Prabhu CPK, Aralekallu S, Sajjan VA, Palanna M, Kumar S, Sannegowda LK (2021) Non-precious cobalt

phthalocyanine-embedded iron ore electrocatalysts for hydrogen evolution reactions. Sustain Energy Fuels 5(5):1448–57

31. FernandoC M, Murilo FC, Sergio ASM, Lucia HM (2008) Electrocatalytic behavior of glassy carbon electrodes modified with multiwalled carbon nanotubes and cobalt phthalocyanine for selective analysis of dopamine in presence of ascorbic acid. Electro Analysis 20:851–857

32. Aralekallu S, Palanna M, Hadimani S, Prabhu CPK, Sajjan VA, Thotiyl MO, Sannegowda LK (2020) Biologically inspired catalyst for electrochemical reduction of hazardous hexavalent chromium. Dalton Trans 49:15061–15071

33. Lokesh KS, Shambhulinga A, Manjunatha N et al (2015) Porphyrin macrocycle-stabilized gold and silver nanoparticles and their application in catalysis of hydrogen peroxide. Dye Pigment 120:155–160

34. Endo K, Katayama Y, Miura T (2005) A rotating disk electrode study on the ammonia oxidation. Electrochim Acta 50:2181–2185

35. Diaz LA, Valenzuela-Muñiz A, Muthuvel M, Botte GG (2013) Analysis of ammonia electro-oxidation kinetics using a rotating disk electrode. Electrochim Acta 89:413–21

36. Rosca V, Koper MTM (2006) Electrocatalytic oxidation of ammonia on Pt(111) and Pt(100) surfaces. Phys Chem Chem Phys 8:2513–2524

37. Palanna M, Aralekallu S, Keshavananda Prabhu C, Sajjan VA, Sannegowda LK (2021) Nanomolar detection of mercury (II) using electropolymerized phthalocyanine film. Electrochim Acta 20(367):137519

38. Dar GN, Umar A, Zaidi SA et al (2012) Ultra-high sensitive ammonia chemical sensor based on ZnO nanopencils. Talanta 89:155–161

39. Khan SB, Rahman MM, Jang ES et al (2011) Special susceptive aqueous ammonia chemi-sensor: extended applications of novel UV-curable polyurethane-clay nanohybrid. Talanta 84:1005–1010

40. Rahman MM, Jamal A, Khan SB, Faisal M (2011) Characterization and applications of as-grown β-Fe2O 3 nanoparticles prepared by hydrothermal method. J Nanoparticle Res 13:3789–3799

41. Rahman MM, Jamal A, Khan SB, Faisal M (2011) CuO Codoped ZnO Based Nanostructured Materials for Sensitive.pdf. ACS Appl Mater Interfaces 3:1346–1351

42. Zoski CG, Leddy J, Bard AJ (2002) Electrochemical methods: fundamentals and applications (Student Solutions Manual), 2nd edn. Wiley, New York

43. Treimer S, Tang A, Johnson DC (2002) A consideration of the application of Koutecký-Levich plots in the diagnoses of charge-transfer mechanisms at rotated disk electrodes. Electroanalysis 14(3):165–171

44. Wang J (2006) Analytical electrochemistry, 3rd edn. Wiley, New York

## Authors and Affiliations

**C. P. Keshavananda Prabhu[1] · Shambhulinga Aralekallu[1] · Manjunatha Palanna[1] · Veeresh Sajjan[1] · B. Renuka[1] · Lokesh Koodlur Sannegowda[1]**

✉ Lokesh Koodlur Sannegowda
kslokesh@vskub.ac.in

[1] Department of Studies in Chemistry, Vijayanagara Sri KrishnadevarayaUniversity, Jnanasagara Campus, Vinayakanagara, Cantonment, Ballari, Karnataka 583105, India